Lawrence Berkeley National Laboratory

Title
Seismic rupture and ground accelerations induced by CO2 injection in the shallow crust

Permalink
https://escholarship.org/uc/item/7fd3j4ds

Author
Cappa, F.

Publication Date
2012-11-15

Seismic rupture and ground accelerations induced by CO_2 injection in the shallow crust

Frédéric Cappa[1,2] and Jonny Rutqvist[1]

[1] *Lawrence Berkeley National Laboratory, Earth Sciences Division, University of California, Berkeley, USA*

[2] *GeoAzur, University of Nice Sophia-Antipolis, Côte d'Azur Observatory, France*

E-mail addresses: cappa@geoazur.unice.fr (F. Cappa); jrutqvist@lbl.gov (J. Rutqvist)

July 23, 2012

SUMMARY

Because of the critically stressed nature of the upper crust, the injection of large volumes of carbon dioxide (CO_2) into shallow geological reservoirs can trigger seismicity and induce ground deformations when the injection increases the fluid pressure in the vicinity of potentially seismic faults. The increased fluid pressure reduces the strength against fault slip, allowing the stored elastic energy to be released in seismic events that can produce felt ground accelerations. Here, we seek to explore the likelihood ground motions induced by a CO_2 injection using hydromechanical modeling with multiphase fluid flow and dynamic rupture, including fault-frictional weakening. We extend the previous work of Cappa & Rutqvist (2011a-b), in which activation of a normal fault at critical stress may be possible for fast rupture nucleating by localized increase in fluid pressure and large decrease in fault friction. In this paper, we include seismic wave propagation generated by the rupture. For our assumed system and injection rate, simulations show that after a few days of injection, a dynamic fault rupture of few centimeters nucleates at the base of the CO_2 reservoir and grows bilaterally, both toward the top of the reservoir and outside. The rupture is asymmetric and affects a larger zone below the reservoir where the rupture is self-propagating (without any further pressure increase) as a result of fault-strength weakening. The acceleration and deceleration of the rupture generate waves and result in ground accelerations (~ 0.1 to 0.6 g) consistent with observed ground motion records. The maximum ground acceleration is obtained near the fault, and horizontal accelerations are generally markedly higher than vertical accelerations.

1. INTRODUCTION

We seek to examine the likelihood of seismic fault rupture and resulting ground accelerations induced by a CO_2 injection in the shallow crust, using hydromechanical modeling with multiphase fluid flow and dynamic rupture. This is motivated by previous results from Cappa & Rutqvist (2011a-b), which showed that injection induced activation could lead to a fast rupture and seismicity associated with a large drop of fault friction. Moreover, several lines of evidence indicate that pre-existing faults found in the upper crust are subject to failure often in response to very small increases in fluid pressure (Zoback & Gorelick 2012). Here, we extend this work by including seismic wave propagation generated by the rupture, to estimate the possible ground accelerations for a range of realistic material parameters and CO_2 injection rates. Our simulations were conducted to intentionally induce fault activation, which occurred at a high reservoir pressure in an unfavorable stress regime. We studied a case in which a normal fault bounds a storage reservoir between two caprocks corresponding to a critical geometrical case for fault activation during CO_2 injection (Hawkes *et al.* 2004). It is an extreme case that in practice could be avoided by careful site characterizations, monitoring and injection control.

Here, we present 2D simulations of dynamic rupture on a critically stressed normal fault subjected to slow hydromechanical loading related to a localized CO_2 injection. The simulations resolve the aseismic quasi-static deformation (i.e., interseismic phase) and the subsequent dynamic rupture event (i.e., coseismic phase). We use fault-frictional weakening, as supported by many laboratory experiments (Marone *et al.* 2009). Our model simulations show how CO_2 injection may trigger and propagate a seismic rupture

along a fault and generate ground motion, which remains poorly understood despite its importance in the seismic hazard assessment related to CO_2 geological sequestration.

2. NUMERICAL SET-UP

We use the coupled thermo-hydro-mechanical code TOUGH-FLAC, which is described in Rutqvist *et al.* (2002), and previously applied to study fault rupture related to multiphase fluid flow and crustal deformations (Rutqvist *et al*. 2007; Cappa *et al*. 2009; Cappa & Rutqvist 2011a-b). TOUGH2 is a finite-volume code for the simulation of multiphase fluid flow, and FLAC^{3D} is a finite-difference code for the simulation of rupture and wave propagation. In this study, a normal fault with a dip angle of 80° and width of 2.5 m is represented in a 2D plane-strain model (2 km × 2 km) composed of a storage formation 100 m thick, bounded at the top and bottom by a low-permeability 150 m thick caprock, which, in turn, is surrounded by two other permeable formations. The fault and the injection point are spaced 500 m apart horizontally. In this case, we envision a fault with an offset of 125 m, so that the offset will laterally limit the reservoir.

In the simulations, CO_2 is injected as a point source at 1000 m depth with a constant rate of 0.02 kg/m/s (i.e. 630.72 tons/m/year) (Fig. 1). This is the injection rate for the half symmetric model and per meter normal to the 2D model. This injection rate is consistent with that used in previous studies (Rutqvist *et al.* 2007; Cappa & Rutqvist 2011a-b) and is intended to produce an aggressive rate of reservoir pressure increase that would lead to fault activation within few months of injection. However, we may relate this injection rate to a field situation. For example, assuming that injection would take place in a 1 km long horizontal well, the total injection rate for that well would be $630.72 \times 2 \times 1000 \approx$

1.26×10^6 tons/year, i.e. about 1.3 million tons per year. We may also relate this to real injection rates at the In Salah CO_2 storage project, where injection rates have been 0.5 to 1.0 million tons per year distributed over 3 horizontal injection wells, each 1 to 1.5 km long (Rutqvist *et al*. 2010).

At 1000 m depth, initial fluid pressure and temperature (P = 9.81 MPa and T = 35 °C) assure supercritical conditions for CO_2. The temperature is assumed to follow a depth gradient of 25°C/km, assuming a temperature of 10°C at the ground surface. The initial fluid pressure follows a hydrostatic gradient (9.81 MPa/km) and atmospheric pressure of 0.1 MPa at the ground surface. Constant pressure, saturation, and temperature conditions are assumed at the boundaries, except for the left boundary, where no flow occurs. Simulations are conducted in an isothermal mode, which implies that the thermal gradient was maintained according to initial conditions. Null displacement conditions were set normal to the left and bottom boundaries, whereas the top boundary was free to move and stress was set to the right boundary. The model is initially subjected to an extensional stress regime of $\sigma_h = 0.7\sigma_v$ in order to simulate a near-critical stress regime for fault activation (Cappa & Rutqvist 2011a). The stresses increase with depth due to gravity.

Properties for the permeable formations and the caprocks represent sandstone and shale, respectively (Table 1). The medium has P-wave velocity C_P = 2360 m/s, S-wave velocity C_S = 1402 m/s, and density ρ = 2260 kg/m^3. Reservoir rocks are considered to be elastic, whereas elasto-plastic behavior is considered for the fault, including an anisotropic Mohr-Coulomb model (ubiquitous joints presented in Cappa & Rutqvist 2011a-b). The fault has no cohesion. We use (1) a linear strain-softening formulation, in which the coefficient of friction decays linearly from a peak static value, μ_s = 0.6, to a

dynamic value, $\mu_d = 0.2$, over a critical strain of 10^{-3}; and (2) a permeability model in which permeability changes with volumetric strain and porosity according to Rutqvist & Cappa (2011a-b), though we adopt a zero dilation angle for the fault. This implies that permeability can change as a result of changes in effective stress and volumetric strain, but there is no shear-induced permeability change along the fault. Fault hydraulic and mechanical properties are taken from the literature (Wibberley & Shimamoto 2003; Faulkner *et al.* 2006; Cappa *et al.* 2007; Guglielmi *et al.* 2008) and their influence on the fault rupture was previously evaluated in Cappa & Rutqvist (2011*a*). Notably, they showed that the size of the rupture area depends on the initial horizontal-to-vertical stress ratio and fault permeability, which strongly influences the size of the pressurized area, and subsequent stress variations.

We explicitly considered multiphase fluids in this study. The fluid-property module ECO2N (Pruess & Spycher 2007) was employed for modeling the thermodynamic and thermophysical properties of water-NaCl-CO_2 mixtures. The relative permeability of gas and liquid phases is calculated from Corey's function (Corey 1954), while capillary pressure is governed by van Genuchten's function (van Genutchen 1980).

Since our simulations fully account for inertial effects and capture the smooth transition between the quasi-static phase and dynamic rupture, defining the beginning of the dynamic phase is not simple. We use the criterion based on the difference between shear stress (τ) and strength ($c+\mu(\sigma_n-p)$, where c is cohesion, μ is friction coefficient, σ_n is normal stress and p is fluid pressure) along the fault and onset the dynamic phase when this difference is equal or less than 0.1 MPa. This approach allows us to adequately capture the transition. With this scheme, the inertial term is negligible at the time of the

switch, and the transition between the two modes is smooth. The dynamic mode is activated some seconds before the rupture, with the time step reduced to a minimum value ($\delta t \sim \Delta x_{min/} C_P \sim 10^{-4}$ s; with Δx being the distance between two neighbor nodes).

To avoid spurious artificial reflections from the boundaries, absorbing boundary conditions (Perfectly Matched Layer, PML) surround the model, except at the free surface. We discretize the model by rectangular mesh. The edge length on the fault is 0.25 m within the ruptured area in order to ensure that there is enough cells to resolve well the weakening process over the nucleation zone size (R_0). In this study, R_0 is defined as in Templeton *et al.* (2010). Outside the ruptured area, the mesh spacing increases progressively to 5 m. We found that such a mesh refinement was sufficient to avoid mesh-induced artificial reflections.

3. RESULTS

Simulation results show that an abrupt stress drop and subsequent fault slip occurs after 40 days of CO_2 injection (Figs. 2a-3). At the initiation of rupture, the fluid pressure buildup is mainly located in the reservoir, at the contact with caprocks and the fault, whereas the CO_2 is mainly situated near the injection point (Fig. 2b-c). Fluid pressurization (~ 7.5 MPa) induces intense plastic shear strain distributed over a length of about 290 m with a maximum value of 4.5×10^{-3}, in a portion of the fault just below the reservoir (red zone in Fig. 3a). The mean stress drop over the ruptured area is 0.316 MPa; a value within the typical range (0.1 to 100 MPa) for moderate and large earthquakes (Griffith *et al.* 2009). The ruptured zone affects both the fault portion inside the reservoir, where the fluid pressure increases, as well as a large portion of the fault below the

reservoir, where stresses increase due to the forcing imposed by the expanding reservoir. Such behavior is consistent with others studies of fault dynamic rupture, in which nucleation and propagation is not only restricted by the fluid pressure increase, but can also occur by local increases in shear stress (Ampuero *et al.* 2006; Viesca & Rice 2012). Figure 3a also shows that the rupture is bilateral and asymmetric around the nucleation zone located at the base of the reservoir. We showed in a previous study (Cappa & Rutqvist 2011a) that the size of the rupture depends on whether the initial stress ratio (σ_h/σ_v) is close to its frictional limit, and on the imposed fluid pressure.

Figure 3b presents representative time histories of slip and slip velocity at different points on the fault. The rupture initiates at the base of the reservoir as a result of local high fluid pressure, and grows rapidly. The slip grows gradually in and outside the pressurized zone and propagates dynamically. Because the strength of the fault weakens with slip, rupture can propagate outside the reservoir without any further fluid pressure increase. Over the ruptured zone, the slip magnitude ranges between 0.1 and 4.2 cm from the tip to the center (Fig. 3a). The rupture occurs over about 0.2 seconds and propagates at an average velocity of 830 m/s ($\sim 0.6 C_S$). The slip velocity increases instantaneously over a time period of about 0.035s and then decreases progressively. A slope discontinuity of the slip velocity appears shortly after the peak, probably coinciding with the slope discontinuity in the strain-weakening friction law. High-frequency oscillations are visible during the deceleration in the slip velocity time series. These oscillations are probably related to the finite-difference method used in this study. Indeed, de la Puente *et al.* (2009) and Pelties et al. (2012) showed that the finite-difference method suffers from spurious amplified high-frequency oscillations of the slip velocity that commonly occur

in numerical solutions of dynamic rupture problems. Several approaches have been proposed to reduce these oscillations, but they remain an unsolved artificial nuisance for the finite-difference method and other methods unless some artificial damping term is used, except in the Discontinuous Galerkin method, which does not generate spurious high-frequency perturbations due to using a dissipative flux computation (Pelties *et al.* 2012).

From these simulation results, we can calculate the seismic moment ($M_0 = \mu A d$) from the mean slip ($d = 0.03$ cm) over the ruptured area (A), the rock shear modulus ($\mu = 4$ GPa) and a magnitude of an earthquake by $M = (log_{10}\ M_0\ /\ 1.5) - 10.73$ (Kanomori & Anderson 1975). Since our simulations are conducted in a plane-strain model, we can assume a unit lateral extent for rupture (i.e., L = 1 km). Thus, a seismic moment of $M_0 = 4 \times 10^9 \times 1000 \times 290 \times 0.03 = 3.48 \times 10^{13}$ Nm, and a magnitude of $M = 2.96$, are estimated for the rupture induced by the CO_2 injection simulated here, at 500 m from the fault. We recognized that our calculated magnitudes depend on the assumed 1 km lateral extent of the rupture. This assumed rupture extent is uncertain, but could be related to for example the length of a horizontal injection well.

Figure 4 shows synthetic seismograms and Fourier acceleration spectra at two stations set on the ground surface, respectively at the center of the reservoir and on top of the fault. The ground motions are nearly identical with a first arrival at t=0.5 s that corresponds to the passing P-waves, and a second large peak at t=0.8 s that corresponds to the passing S-waves generated by the rupture. The second peak shows a substantial acceleration. The peak horizontal ground acceleration is higher than the vertical component, with the highest acceleration (~0.6g) obtained near the fault. The acceleration

and deceleration of the rupture generate waves and result in ground accelerations that increase gradually until 30 Hz, and then a sharp slope discontinuity marks a decrease at high frequency (Fig. 4e-f). The increasing acceleration over the first 30 Hz is due to a directivity effect of the bilateral rupture. The high-frequency oscillations are likely related to the acceleration and deceleration of the rupture, and the interaction of the waves with fluids. A marked feature of the acceleration spectra is the much higher frequency content (short bursts of energetic signals on the orange curves) of the vertical component compared to the horizontal ones. We should clarify that, since our simulation includes plasticity, the energy dissipated by the plastic response of the fault reduces the ground accelerations compared to those calculated in a purely elastic medium. Such behavior was also shown in Templeton *et al.* (2010) for the study of ground motions induced by dynamic rupture with off-fault plasticity.

4. CONCLUSION

We have investigated fault activation by CO_2 injection and resulting ground accelerations, using numerical simulations that include both multiphase fluid flow and strain-weakening fault friction over a cycle of slow hydromechanical loading followed by dynamic rupture. Here we intentionally simulated a critical case involving the injection-induced fluid-pressure increase that penetrates a fault with an initial tectonic stress field near its frictional limit for shear rupture. Our results showed that a CO_2 injection into the crust can induce a pressurized region that spreads at the pace of the fluid diffusion and can lead to dynamic slip along pre-existing faults. In our models, the fault rupture initiates at the base of the reservoir as a result of local high pressure, and then grows

dynamically outside the reservoir without any further increase in fluid pressure, because the fault strength weakens with slip. The rupture is bilateral and asymmetric, and generates ground accelerations with a difference in the frequency content of the vertical and horizontal components.

Finally, the present study provides the basic framework upon which the investigation of different fault geometries and frictional behavior can be built. During a CO_2 injection, faults may be subjected to cyclic deformations with phases of fluid accumulation and phases of rupture. For instance, the seismicity induced by such a cycle can be composed of numerous microearthquakes over a long period of time, as observed at the Weyburn CO_2 pilot site (Canada), from 2004 to 2010, with less than 100 microseismic events having magnitudes of -1 to -3 (Verdon *et al.* 2011). Thus, for further numerical investigations of seismicity induced by CO_2 injection into faulted reservoirs, we will attempt to link fluid flow and mechanical stresses with the more advanced rate-and-state friction law, which describes the entire friction evolution over several cycles of rupture, with friction increasing with slip velocity before falling to low dynamic levels.

simulation of dynamic rupture. We also thank the three anonymous reviewers for their constructive comments and suggestions that improved our paper.

REFERENCES

Ampuero, J.P., Ripperger, J., & Mai, P. M., 2006. Properties of dynamic earthquake ruptures with hetergeneous stress drop, in *Radiated Energy and the Physics of Earthquakes, edited by A. McGarr, R. E. Abercrombie, H. Kanamori, and G. Di Toro*, pp. 255-261, Geophysical Monograph Series 170, American Geophysical Union, Washington D.C.

Cappa, F., Guglielmi, Y., & J. Virieux, 2007. Stress and fluid transfer in a fault zone due to overpressures in the seismogenic crust, *Geophys. Res. Lett.*, 34, L05301, doi:10.1029/2006GL028980.

Cappa, F., Rutqvist, J., & Yamamoto, K., 2009. Modeling crustal deformation and rupture processes related to upwelling of deep CO_2-rich fluids during the 1965–1967 Matsushiro earthquake swarm in Japan, *J. Geophys. Res.*, 114, B10304, doi:10.1029/2009JB006398.

Cappa, F., & Rutqvist, J., 2011a. Impact of CO_2 geological sequestration on the nucleation of earthquakes. *Geophys. Res. Lett.*, 38, L17313, doi:10.1029/2011GL048487.

Cappa, F., & Rutqvist, J., 2011b. Modeling of coupled deformation and permeability evolution during fault reactivation induced by deep underground injection of CO_2. *Int. J. Greenhouse Gas Control*, 5, 336-346, doi:10.1016/j.ijggc.2010.08.005

Corey, A.T., 1954. The interrelation between oil and gas relative permeabilities. *Producers Monthly*, 38-41.

de la Puente, J., Ampuero, J.P., & Kaeser, M., 2009. Dynamic rupture modeling on unstructured meshes using a discontinuous Galerkin method. *J. Geophys. Res.*, 114, B10302, doi:10.1029/2008JB006271

Kanamori, H., & Anderson, D.L., 1975. Theoretical basis of some empirical relations in seismology, *Bull. Seism. Soc. Am.*, 65, 1073-1095.

Faulkner, D.R., Mitchell, T.M., Healy, D., & Heap, M., 2006. Slip on 'weak' faults by the rotation of regional stress in the fracture damage zone, *Nature*, 444(7121):922-925.

Griffith, W.A., Di Toro, G., Pennacchioni, G., Pollard, D.D., and Nielsen, S., 2009. Static stress drop associated with brittle slip events on exhumed faults, *J. Geophys. Res*., 114, B02402, doi:10.1029/2008JB005879.

Guglielmi, Y., Cappa, F., & Amitrano, D., 2008. High-definition analysis of fluid-induced seismicity related to the mesoscale hydromechanical properties of a fault zone, *Geophys. Res. Lett.*, *35*, L06306, doi:10.1029/2007GL033087.

Hawkes, C.D., McLellan, P.J., Zimmer, U., & Bachu, S., 2004. Geomechanical factors affecting geological storage of CO_2 in depleted oil and gas reservoirs: risks and mechanisms. In: *Proceedings of Gulf Rocks 2004, the 6th North America Rock Mechanics Symposium (NARMS): Rock Mechanics Across Borders and Disciplines*, Houston, Texas.

Marone, C., Cocco, M., Richardson, E., & Tinti, E., 2009. The critical slip distance for seismic and aseismic fault zones of finite width, *In: Fault-zone Properties and Earthquake Rupture Dynamics, edited by E. Fukuyama, International Geophysics Series*, 94, 135-162, Elsevier.

Pelties, C., De La Puente, J., Ampuero, J.P., Brietzke, G., & Kaeser, M., 2012. Three-dimensional dynamic rupture simulation with a high-order Discontinuous Galerkin method on unstructured tetrahedral meshes. *J. Geophys. Res.*, 117, B02309, doi:10.1029/2011JB008857.

Pruess, K., & Spycher, N., 2007. ECO2N – A fluid property module for the TOUGH2 code for studies of CO_2 storage in saline aquifers, *Energ. Conv. Man.*, doi:10.1016/j.enconman.2007.01.016.

Rutqvist, J., Wu, Y-S., Tsang, C-F., & Bodvarsson, G., 2002. A modeling approach for analysis of coupled multiphase fluid flow, heat transfer, and deformation in fractured porous rock, *Int. J. Rock Mech. Min. Sci.*, 39:429-442.

Rutqvist J., Birkholzer J.T., Cappa F., & Tsang C-F., 2007. Estimating maximum sustainable injection pressure during geological sequestration of CO_2 using coupled fluid flow and geomechanical fault-slip analysis. *Energy Conv. Man.,* 47:1798-1807.

Rutqvist J., Vasco D., & Myer L., 2010. Coupled reservoir-geomechanical analysis of CO_2 injection and ground deformations at In Salah, Algeria. *Int. J. Greenhouse Gas Control*, 4, 225–230.

Templeton, E.L., Bhat, H.S, Dmowska, R., & Rice, J.R., 2010. Dynamic rupture through a branched fault configuration at Yucca Mountain, and resulting ground motions. *Bull. Seism. Soc. Am.*, 100(4):1485-1497, doi:10.1785/0120090121.

van Genuchten, M.T., 1980. A closed-form equation for predicting the hydraulic conductivity of unsaturated soils, *Soil. Sci. Soc. Am. J.*, 44:892-898.

Verdon, P.P., Kendall, J.M, White, D.J., & Angus, D.A., 2011. Linking microseismic event observations with geomechanical models to minimize the risks of storing CO_2 in geological formations. *Earth Planet. Sci. Lett.,* 305:143-152.

Viesca, R.C, & Rice, J.R., 2012. Nucleation of slip-weakening rupture instability in landslides by localized increase of pore pressure. *J. Geophys. Res.*, in press

Wibberley, C.A.J, & Shimamoto, T., 2003. Internal structure and permeability of major strike-slip fault zones : the Median Tectonic Line in Mie Prefecture, Southwest Japan, *J. Struct. Geol.*, 25:59-78.

Zoback, M.D., & Gorelick, S.M., 2012. Earthquake triggering and large-scale geologic storage of carbon dioxide, *Proceedings of the National Academy of Sciences of the United States of America*, doi:10.1073/pnas.1202473109

Table 1. Material parameters

Parameters	Storage Formation	Caprock	Others Formations	Fault
Young's modulus	10 GPa	10 GPa	10 GPa	5 GPa
Poisson' ratio	0.25	0.25	0.25	0.25
Porosity	0.1	0.01	0.1	0.1
Permeability	$10^{-13}\,m^2$	$10^{-19}\,m^2$	$10^{-14}\,m^2$	$10^{-16}\,m^2$
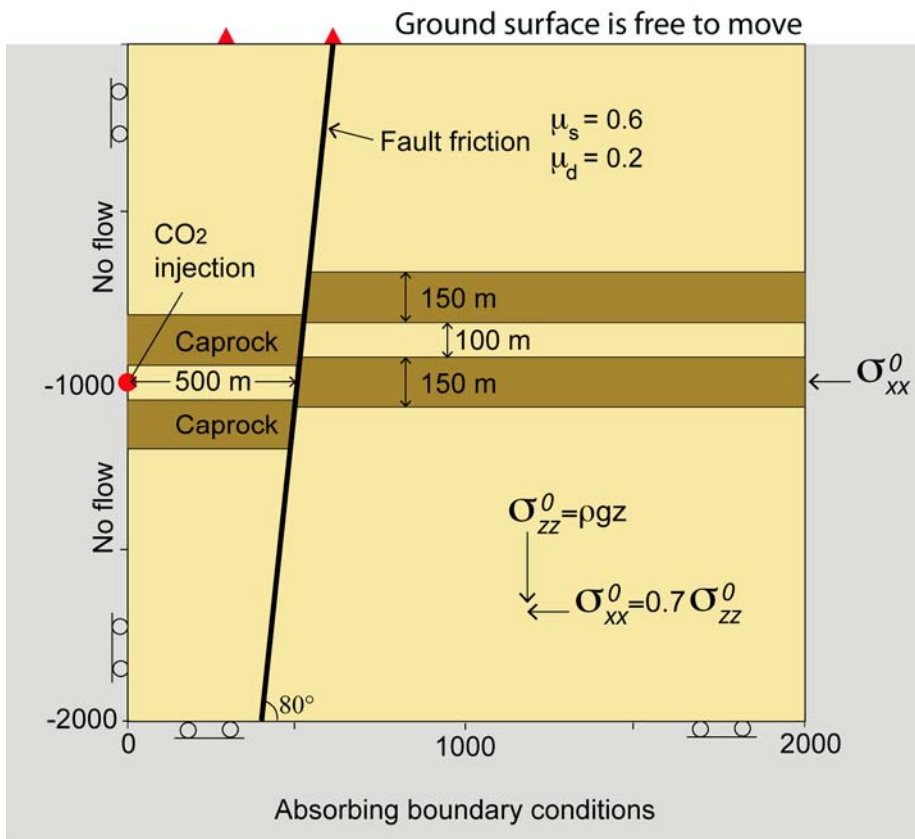
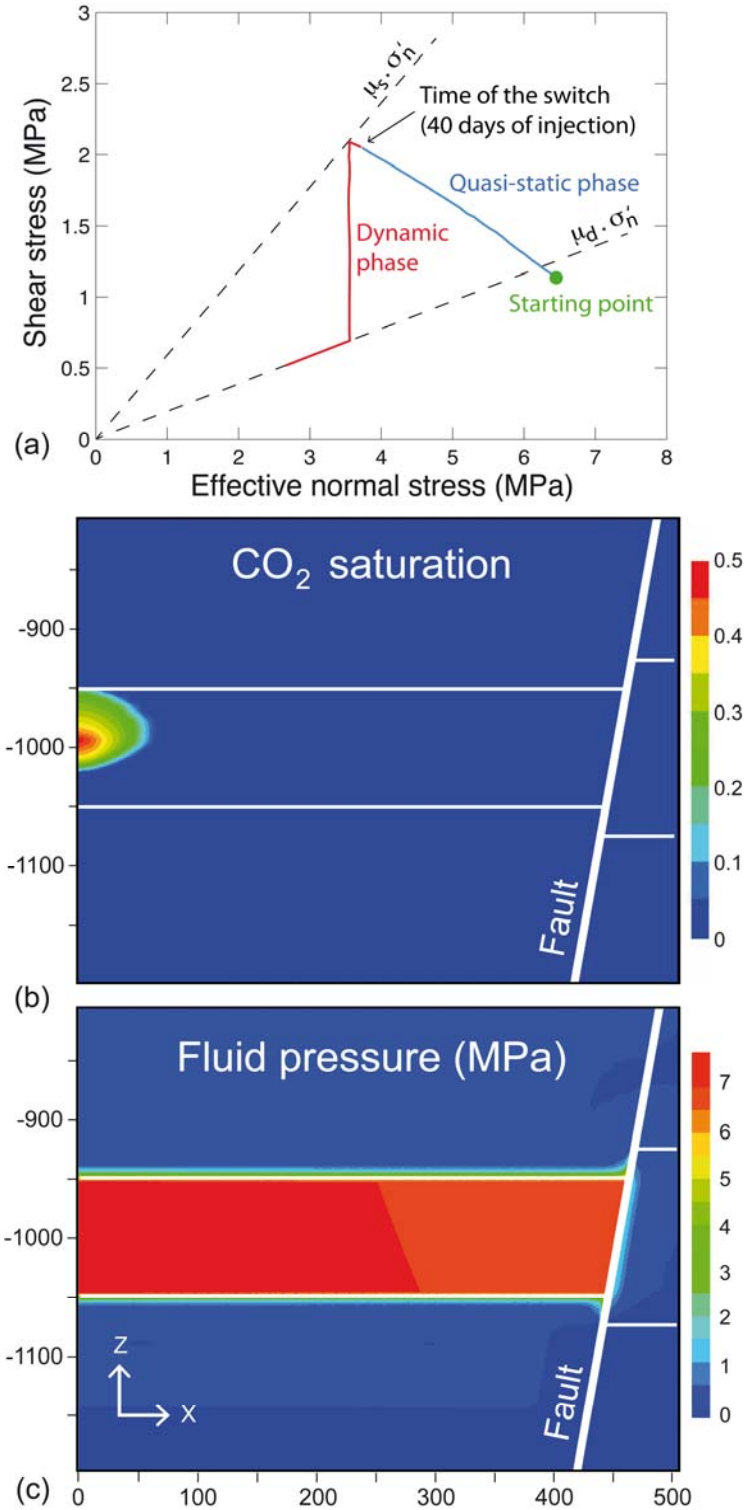**Figure 1.** (a) Model geometry and position of control points (red triangles) for ground accelerations.

Figure 2. (a) Shear stress-versus-effective normal stress path in the nucleation zone (control point 5 in Figure 3a) of the rupture within the fault (the slow quasi-static phase is in blue and the dynamic phase is in red). Snapshots of change in (b) CO_2 saturation and (c) fluid pressure in the reservoir at the time of seismic rupture.
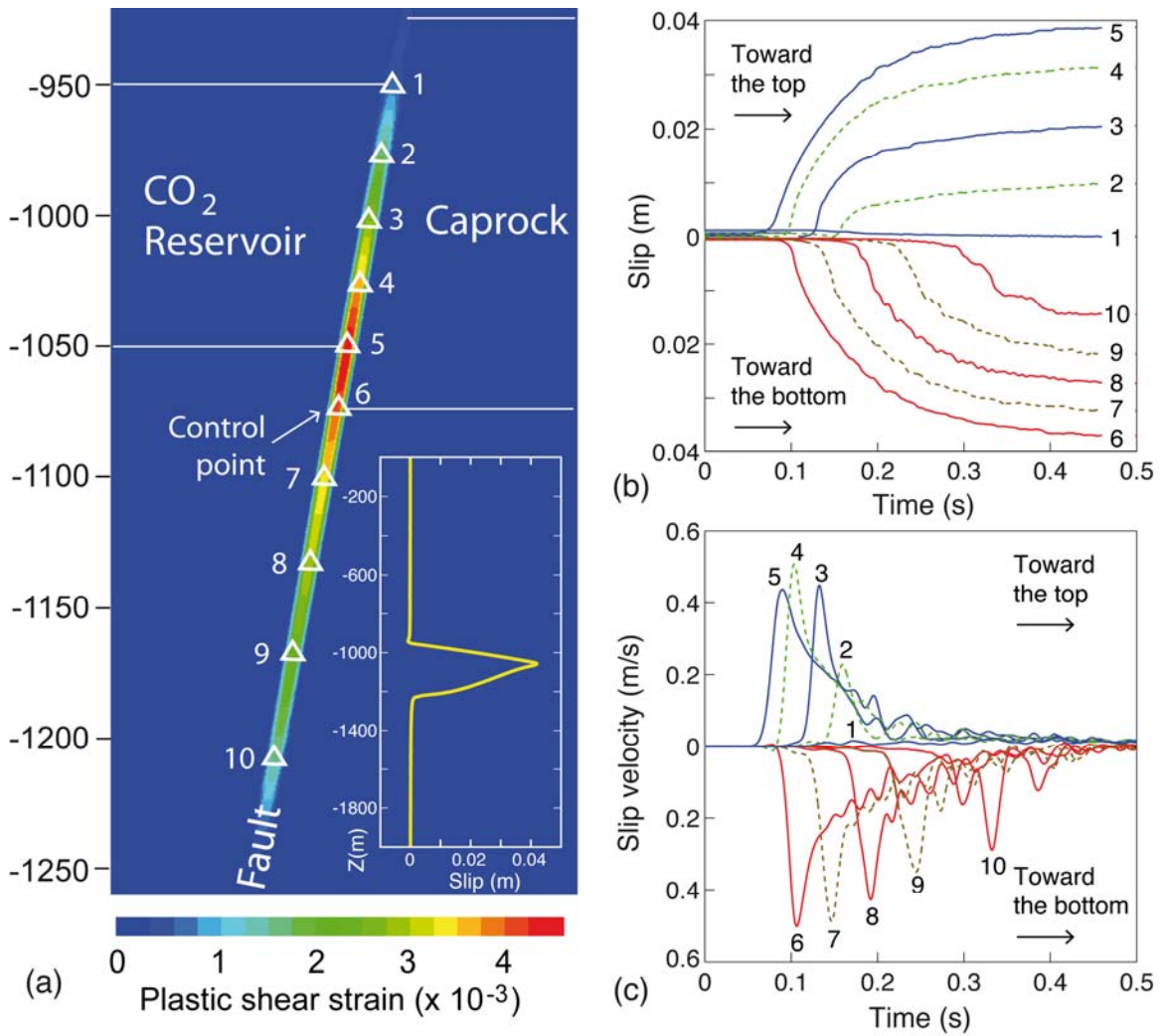
Figure 3. (a) Plastic shear strain in the ruptured area and slip profile at the time of seismic rupture, and evolution of (b) slip and (c) slip velocity as function of time at different control points along the fault (white triangles on (a)). The rupture starts at the bottom of the CO_2 reservoir, near the control point 5.
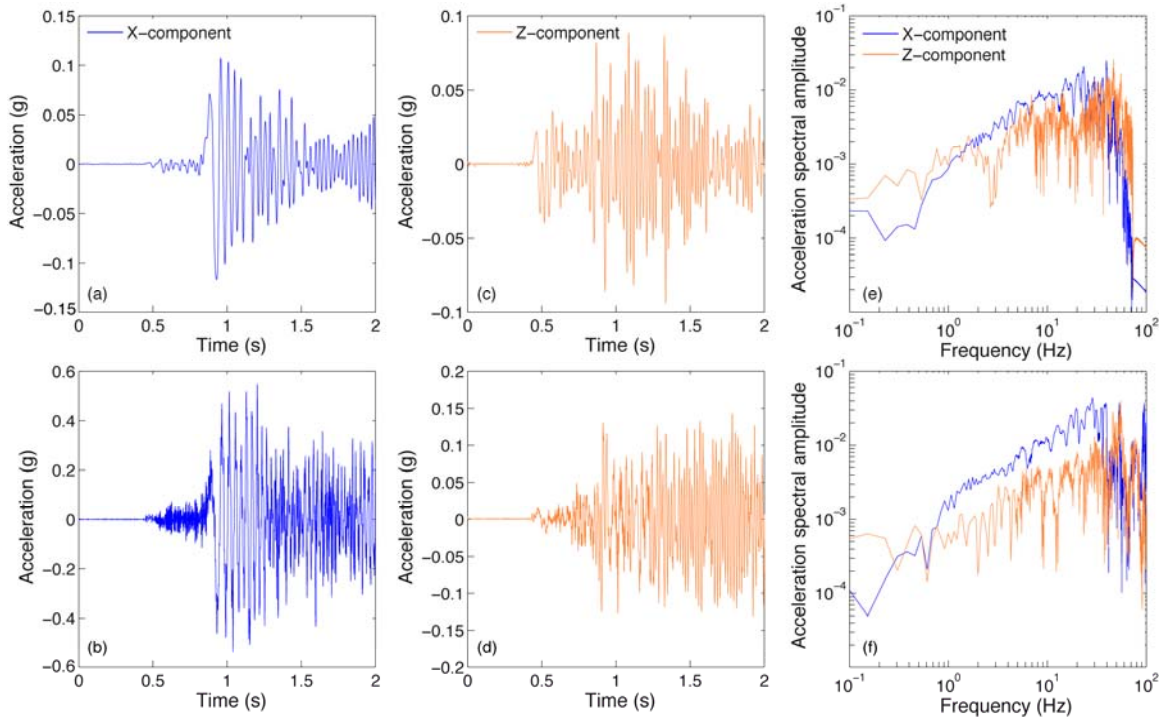
Figure 4. (a-b) Horizontal and (c-d) vertical components of accelerations at the ground surface, and (e-f) Fourier amplitude spectra at two measuring points (see red triangles on Fig. 1): (top) at the reservoir centre (x=330, z=0), (bottom) on top of the fault (x=660, z=0).